This is a preprint, the final version is subject to change, of the American Mineralogist (MSA)
Cite as Authors (Year) Title. American Mineralogist, in press.
(DOI will not work until issue is live.) DOI: http://dx.doi.org/10.2138/am-2015-5170

Three-component mixed-layer illite-smectite-kaolinite (I/S/K) minerals in hydromorphic soils, south China

HANLIE HONG[1,2]*, FENG CHENG[2], KE YIN[2], GORDON JOCK CHURCHMAN[3] AND CHAOWEN WANG[2]

(*[1]Key Laboratory of Geobiology and Environmental Geology, the Ministry of Education, China University of Geosciences, Wuhan, Hubei, 430074; [2]Faculty of Earth Sciences, China University of Geosciences, Wuhan, Hubei, 430074; [3]School of Agriculture, Food and Wine, The University of Adelaide, 5005 Australia*)

ABSTRACT

To understand clay mineral transformations in hydromorphic conditions in the red earth sediments in Xuancheng, south China, clay mineralogy was investigated using X-ray diffraction (XRD) and high resolution transmission electron microscopy (HRTEM). The XRD results indicated that clay minerals in the hydromorphic soils were illite, kaolinite, smectite, vermiculite, and mixed-layer illite/smectite and illite/smectite/kaolinite. Changes of the kaolinitic reflections under the various conditions suggested that the kaolinitic phase is a mixed-layer structure having kaolinite layers randomly interstratified with illite and smectite layers. HRTEM observation showed that 10 Å illite layers interstratified with both 15 Å smectite layers and 7 Å kaolinite layers in clay particles, confirming the occurrence of illite/smectite/kaolinite (I/S/K) three-component mixed-layer clays. The lattice fringes of the I/S/K clays appeared corrugated and vanishing, and also exhibited variable thickness along a lattice fringe, which were consistent with changes from illite to

smectite, from smectite to kaolinite, and from illite to kaolinite, respectively. Hydromorphic conditions in the Xuancheng soils led simultaneously to the direct transformation of illite to kaolinite and the transformation of illite to smectite to kaolinite in the pedogenic processes, and the formation of I/S/K three-component mixed-layer clays as intermediate products of these processes.

Key words: I/S/K mixed-layer, hydromorphic soil, net-like red earth; weathering

INTRODUCTION

In supergene weathering processes, the pre–existing clay minerals may transform into other clay species through a sequence of intermediate interstratified species formed prior to the formation of end members with increasing degrees of weathering and changes in climatic conditions (Singer, 1980). During the formation of Alfisols, clay transformation is governed by the mobility of the elements released by mineral dissolution (Chesworth, 1992). Illite is usually formed during diagenesis processes under relatively high temperatures and pressures, and is thermodynamically unstable in soil environments. In soils in moisture regimes where rainfall exceeds evapotranspiration, the percolating water carries out soluble ions such as K^+ and thus induces K^+ depletion in the illitic minerals. However, in soils of alternating moist and dry regimes where there is a distinct dry season, mineral dissolution and water percolation is restricted, and the limited chemical leaching reduces the alteration of illitic mineral (Bertsch and Thomas, 1985).

Alteration of illite in weathering profiles has been most often reported to weather to

vermiculite or hydroxyl-Al interlayered vermiculite (HIV) (Allen and Hajek, 1989; Yin et al., 2013), smectite (Ismail, 1970; Churchman, 1980; Bonifacio et al., 2009; Churchman and Lowe, 2012), and kaolinite (Wilson, 2004). In a few instances it has been reported to weather to mixed-layer illite/smectite (I/S), illite/kaolinite (I/K), illite/vermiculite (I/V), and kaolinite/smectite (K/S) (Hong et al., 2012; 2014; Han et al., 2014). The formation of mixed layer clay minerals of two-component systems is often reported in the weathering process. However, three-component interstratification of the clay minerals in soils has rarely been recognized, as interstratification with three or more components is difficult to detect, in particular, if this phase is present in small amounts in a multiphase sample (Cradwick and Wilson, 1978). The calculated XRD pattern method provided a helpful approach to recognize three-component mixed-layer species in soils, and more and more results have proven that three-component mixed-layer clay minerals in soils are much more common than originally thought (Cradwick and Wilson, 1978; Sakharov et al., 1999; Hubert et al., 2012; Dumon et al., 2014).

In the mid-lower reaches of the Yangtze River, south China, Quaternary red earth sediments occur widely in the hills, terraces, coalesced alluvial pans, and parts of the piedmont belts, with a characteristic net-like vein texture in the lower portion of the soil profile. A recent geochemical and isotopic study showed that the sediments have efficiently recycled materials of old fluvial deposits of the drainage basins of the mid-lower Yangtze River, and have subsequently undergone intense chemical weathering (Hong et al., 2013). It is generally accepted that the formation of red earth

sediments with a net-like vein texture was linked to hydromorphic conditions during pedogenic processes (Brinkman, 1970; Zhu, 1988; Li and Gu, 1997 ; Hong et al., 2010). Therefore, in addition to podzolisation and lessivage processes, weathering of illite in the net-like horizon of the soil profile will also be affected by hydromorphic conditions. Hydromorphism is characterized by redox processes, which have a direct effect on the solubilisation of Fe and Mn oxides and hydroxides, and also affect layer silicates through a variation in their charge (Stucki, 2006). Seasonal drying may also concentrate hydrogen ions, lowering the pH of the soil solutions and solubilizing aluminium. Thus, unusual patterns of illite alteration could probably be expected. The purpose of this investigation was to characterize the transformations that have occurred to illite minerals because of the distinct soil processes and therefore, to shed more light on illite alteration in supergene weathering and gain a better understanding of the processes of formation of the soils.

MATERIALS AND METHODS

The Xuancheng soil profile and sampling

The studied area is located in Xuancheng, Anhui Province, in the mid-lower reaches of the Yangtze River, southeastern China (Figure 1). It is in the subtropical climate zone. The position of the Xuancheng soil profile is at 118°51'E, 30°54'N, in the southeast of Xuancheng city, where excavation for palaeoliths provided a well developed vertical profile. The soil profile is situated on the second terrace of the Shuiyang River, a branch of the Yangtze River. The soils are classified as red earths

(on summit and slope) (Gu et al., 2001), consistent with Oxisols in their characteristics.

The soil profile has been described in detail by Hong et al. (2010), and is briefly described here as follows. The thickness of the soil profile is around 10 m, overlaying unconformably a clay gravel layer, in which the gravels are well–rounded, with a size of 5 to 15 cm. The upper portion (0 to 2.2 m) is homogeneously brown to yellow–brown sandy clays. The middle portion (2.2 to 6.3 m) is grey–yellow to red–brown sandy clays, with sporadically light color spots and white small short veins. The lower portion (6.3 to 10.4 m) is brown–yellow to red–brown loamy clays, with distinct net-like texture.

The white net-like veins occur in vertical, horizontal, and irregular orientations and in different shapes between the layers of the soil profile, and make up to ~40% by volume locally in the lower soil profile (Figure 2). White spots in the middle portion usually have a size of 0.3 to 2 cm, and the white net-like veins in the lower portion are usually less than 10 cm long and 3 cm wide, and occasionally fine white veins with 5–25 cm long and 0.1–0.5 cm wide were also observed in this portion. Samples were collected from each portion of the soil profile and detailed clay mineralogical investigation was performed for the lower portion with a distinct white net-like structure, indicative of intense hydromorphism. The physical and chemical properties of the soils with white net-like structure are listed in Table 1. The soils were strongly acidic, with a pH value of 4.91±0.05, similar to those of Latosols (4.5-5.5). However, the CEC value of the net-like red soil was 10.3±0.6 cmol/kg (Hu et al., 1999),

111 significantly larger than that of the Latosols (2.86 cmol/kg) derived from weathering
112 of the underlying basalt in Hainan (Yin et al., 2006). The soils with a distinct white
113 net-like structure contained only trace amounts of organic matter, with a content of
114 0.294±0.087 wt% (Zhao and Yang, 1995). In general, particles with a size >100 μm
115 were hardly observed in the soils, and the sand component (>63 μm) was only present
116 in trace amounts. The most abundant particle size is the silt component (4-63 μm),
117 followed by the clay component (<4 μm), with averaged values of 69.68 % and
118 30.22 %, respectively (Zhu, 2007).
119
120 **X-ray diffraction**
121 The soil samples were air-dried and then crushed and ground manually to powder
122 grain-size with an agate mortar and pestle. To estimate the mineral composition of the
123 soils, randomly oriented bulk samples for XRD analysis were prepared by mounting
124 the powder sample onto a sample plate using the back-pressing method. The clay
125 mineral fractions of the soil samples were obtained using a sedimentation method
126 (Jackson, 1978). The powder sample was first treated by 10% H_2O_2 to remove organic
127 materials and was then washed, transferred into a 1000 ml beaker, and then 1000 ml
128 deionized water was added and stirred for ~120 minutes. The clay suspension was
129 allowed to settle for 60 h. The suspension in the uppermost part of the beaker was
130 moved into a tube, and the clay fraction was collected by centrifugation method. The
131 oriented clay samples were prepared by carefully pipetting the clay suspension onto a
132 glass slide. Ethylene glycol saturation was done by treating the oriented sample in a

sealed glass desiccator with ethylene glycol at 65 °C for 4 h in an electric oven. The oriented clay samples were heated to 400°C and 550°C for 1 h respectively in a Muffle furnace to determine the dehydration reaction of clay species. The clay fractions had been saturated with K^+ and Mg^{2+}, which was performed by adding the air–dried clay fraction into 1 M KCl and 1 M $MgCl_2$ solutions in each glass tube, and were equilibrated at 50 ºC for 12 hours and then washed with deionized water.

The XRD analyses were performed on a Panalytical X'Pert PRO DY2198 diffractometer at the Laboratory of Geological Process and Mineral Resources, China University of Geosciences (Wuhan). The instrument was operated at 40 kV and 35 mA with Ni-filtered Cu Kα radiation, and the slit conditions of 1° divergence slit, 1° anti-scatter slit, and 0.3 mm receiving slit. The XRD patterns were collected from 3° to 60° 2θ at a scan rate of 4° 2θ/min with a step size of 0.02º 2θ

HRTEM analysis

Both the air-dried clays and the glycolated clays were prepared for HRTEM analysis in order to obtain better understanding of their interlayer characteristics. The clay samples were air-dried at ambient temperature, and then embedded in M-bond 610 resin between two glass slides to obtain highly oriented clay particles; the resin embedded clay sample was then solidified in an electric oven at 80 ºC for 2 h. For HRTEM observation, a thin section was cut vertically from the glass slides so that the (001) plane of clay particles was preferentially oriented. HRTEM observation was undertaken on a Tecnai G2 20 S-TWIN high resolution transmission electron

155 microscope equipped with a GENESIS 2000 X-ray energy dispersive detector (EDS),
156 at the Key Laboratory of Catalysis and Materials Science of the State Ethnic Affairs
157 Commission and Ministry of Education, South-Central University for Nationalities.
158 The instrument was operated at an accelerating voltage of 160 kV. The beam spot size
159 was 1.5 nm, and the point resolution and the line resolution were 0.24 nm and 0.14
160 nm respectively.

161 The lattice fringe images were obtained under over-focus conditions in order to
162 obtain the best contrast effect of lattice fringes of clay particles (Guthrie and Veblen,
163 1989). In our observation, only lattice fringes of the 001 reflection were obtained with
164 a 10-μm diameter objective aperture, and the EDS microanalysis of the crystal domain
165 of clay minerals was undertaken in TEM mode only after taking the lattice-fringe
166 images.

167

168 **RESULTS**

169 **X–ray diffraction**

170 The XRD results showed that mineral components of the soils were quartz, clay
171 minerals, and minor feldspars. Smectite, vermiculite, and illite were identified using
172 the 15.0 Å, 14.5 Å and 10.0 Å reflections, and kaolinite was determined by the 001
173 and 002 reflections of 7.2 Å and 3.58 Å. Mixed-layer K/S was characterized by the
174 ~7.5 Å peak, and mixed-layer I/S had a basal 001 spacing of mainly ~12 Å, displaying
175 a relatively broad 001 peak. Clay minerals in the soil samples were illite, kaolinite,
176 smectite, vermiculite, and illite/smectite (R0) and kaolinite/smectite (R0) mixed-layer

177 clays (Figure 3a). The relative proportions of clay minerals changed markedly
178 between the soil samples based on their relative intensities of characteristic peaks of
179 the clay species. The upper portion contained more illite but less kaolinite, vermiculite,
180 and mixed-layer illite/smectite compared to the middle portion. The contents of
181 kaolinite, vermiculite, and mixed-layer illite/smectite increased while that of illite
182 decreased in the middle portion; mixed-layer kaolinite/smectite occurred abundantly
183 in this portion. The lower portion had more kaolinite, smectite, and mixed-layer
184 illite/smectite but less illite relative to the upper and middle portions.

185 Clay species in the soil sample from the white net-like structure portion were
186 identified as illite and kaolinite, with minor smectite, vermiculite, and mixed-layer
187 illite–smectite (Figure 3b). On glycol saturation the broad peak at ~13 Å in air–dried
188 conditions disappeared and a 14.1 Å peak was present. The ~15 Å peak expanded to
189 17.2 Å, suggesting the presence of small amounts of smectite. For air-dried specimen,
190 the kaolinitic phase had *d*(001) of 7.20 Å and *d*(002) of 3.57 Å, respectively. When
191 saturated with Mg^{2+} the *d*(001) and and *d*(002) of this phase were 7.39 Å and 3.58 Å,
192 in association with a notable increase in intensity of the 4.17 Å peak, and the ~13 Å
193 broad peak decomposed into 14.4 Å and 10.1 Å peaks, while the 4.99 Å peak
194 decomposed into 4.99 Å and 4.92 Å peaks respectively. Glycolation of the
195 Mg^{2+}-saturated sample caused the expansion of 14.4 Å to 16.9 Å and an increase in
196 intensity of the 10 Å peak. The occurrence of 14.4 Å and 4.92 Å peaks after Mg^{2+}
197 saturation indicated that the clay species was enriched in an illitic phase associated
198 with randomly interstratified smectite/illite (Laird and Nater, 1993). The *d*(001) of

7.39 Å and *d*(002) of 3.58 Å of kaolinite phase of the Mg^{2+}-saturated specimen were different from those of pure kaolinite, which may be due to partial overlapping of these reflections with the nearest I-S-K reflections, and the kaolinitic phase is a mixed-layer structure having kaolinite layers randomly interstratified with illite and smectite layers (Sakharov et al., 1999).

The 14.9 Å and 12.8 Å peaks disappeared and the intensity of the 10 Å peak significantly increased after K^+–saturation, indicating that the intercalated components in smectite mineral and the smectite layers of the I/S clay were replaced by the K^+ cation. When heated to 400 °C, both the 14.9 Å and 12.8 Å peaks collapsed to 10 Å and its intensity largely increased relative to those of the air–dried and glycolated samples, and with further heating to 550 °C, the 7.2 Å peak of kaolinite disappeared, while the intensity of 10 Å peak increased markedly. The complete collapse to 10 Å under K^+–saturation with heating treatments at 400 °C and 550 °C reinforced that the expandable layers are smectitic in nature.

HRTEM observation

Clay particles were present in three distinct different morphologies under HRTEM observation. Most of the clay grains showed near-perfect crystalline character, occurring as long plate-shaped crystals with a straight outline along the (001) dimension. Some of the particles were wave–shaped with a relatively thin and poorly developed (001) surface, which are characteristic morphologies of smectites and mixed-layer illite-smectites (Figure 4a; Van Der Gaast et al., 1986; Deconinck and

Chamley, 1995). Less commonly, clay particles occur as aggregates with a small grain size and irregular outlines (Figure 4b). Usually, crystal boundaries of the clay particles could be readily identified and their lattice fringes were well–defined. However, for clay particles with small sizes, lattice fringe images were difficult to obtain due to the structural damage from dehydration caused by the electron beam heating.

Clay particles with relatively thick and plate-shaped outline usually exhibited straight lattice fringes with 10 Å spacing, consistent with those of illite layers. Some of the clay particles showed homogeneous 10 Å fringes and were indicative of discrete illite grains (Figure 4c). In clay particles with relatively thin and wave–shaped outlines, only 15 Å fringes were observed, indicative of discrete smectite particles. However, in some clay crystals, the 10 Å layers were irregularly interstratified with both 15 Å and 7 Å layers (Figure 4d). The 10 Å and 15 Å fringes were probably derived from illite and smectite layers respectively, while the 7 Å fringe was probably derived from kaolinite layer. The I/S/K lattice–fringe sequences displayed a disordered structure, and were randomly interstratified according to HRTEM observation.

The interstratified illite, smectite, and kaolinite layers in the clay particles suggested that illite transformed into I/S/K three component mixed-layer clays (Figure 4e). In general, the illite–smectite–kaolinite mixed–layer clays were characterized by interstratified lattice fringes of 10 Å, 15 Å, and 7 Å under HRTEM observation. Most lattice fringes of the clay layers were wave-shaped while some were straight and were

243 relatively well-defined. The white fringes appeared corrugated and vanishing in some
244 parts, and sometimes the fringes showed variable thickness, with a spacing changing
245 from 15 Å to 7 Å, and with crystal boundaries, although layer terminations within the
246 crystals were not aligned. In the glycolated sample, the clay particles were also clearly
247 observed to be composed of three kinds of crystal domains with lattice-fringe
248 spacings of 10 Å, 17 Å, and 7 Å (Figure 4e), consistent with illite, smectite, and
249 kaolinite layers respectively, which appeared as a three component composite instead
250 of an interstratified structure, suggesting a stage in the overall transformation from
251 illite to smectite and kaolinite. The EDS analyses of the 7 Å domain suggested that
252 the area consisted of mainly Si and Al, in good agreement with those of kaolinite
253 (Figure 5a). The chemical composition of the 10 Å area had a significantly high
254 content of K and minor Mg, and relatively less Al compared to those of the 7 Å area,
255 and that of the 17 Å area contained abundant Mg and K, with minor Ca, consistent
256 with those of smectite and illite respectively (Figure 5b,c).
257

258 **DISCUSSION**

259 The XRD evidence suggested that clay minerals in the soil sample from the white
260 net-like structure portion were illite, kaolinite, smectite, and mixed-layer
261 illite–smectite (Figure 3). However, HRTEM lattice-fringe images clearly indicated
262 occurrence of three-component mixed-layer clays. Disordered mixed–layer I/S/K with
263 10 Å illite layers interstratified with 15 Å smectite layers and 7 Å kaolinite layers
264 occurred within the I/S/K crystals (Figure 4d,e). In glycolated samples, the observed

17 Å lattice fringes suggested the occurrence of smectite layers instead of vermiculite layers within the interstratified clays. Unlike the lattice-fringe images of mixed–layer I/V, in which the 14 Å spacing fringes are usually straight and are interstratified with 10 Å fringes, the lattice fringes of the I/S/K clays appeared corrugated and vanishing, and also showed variable thickness along a lattice fringe, in correspondence with a phase change from illite to smectite or from smectite to kaolinite, and sometimes the lattice fringes of illite, smectite, and kaolinite domains all occurred together within a clay particle. These suggested that the alteration of illite during the pedogenic process involves exchange of K^+ by hydrated cations leading to a swelling of the clay mineral, and local dissolution of the smectite layers, causing the formation of kaolinite (Figure 6); hence the processes of transition of illite to smectite and of smectite to kaolinite could simultaneously occur within a clay particle.

Kaolinite is considered as an end-product of pedogenesis. In soil genesis with intense chemical weathering, leaching of base cations and Si from the parent materials followed by recrystallization will generally result in the formation of kaolinite (e.g. Herbillon et al., 1981; Nahon, 1991; Churchman et al., 2010). As suggested by Hao et al. (2010) and Hong et al. (2013), the Xuancheng soils were derived from fluvial sediments consisting of abundant clay minerals in drainage basins of the mid–lower reaches of the Yangtze River. In moderate chemical weathering under neutral to acidic conditions, the inherited illite clay may probably alter into a mixed–layer I/V mineral as an intermediate through release of potassium from the interlayer, and may further transform into smectite as weathering proceeds (Bhattacharyya et al., 2000;

Bonifacio et al., 2009).

Intermediate clay species occurred widely in the red earth sediments in the mid–lower reaches of the Yangtze River. HIV clays were only present in the upper portion of the soil profile with a relatively low degree of weathering (Yin et al., 2013; Han et al., 2014). Mixed-layer I/V only occurred in certain soil layers in the middle soil profile (Hong et al., 2014). Mixed-layer I/S and K/S clays were observed mainly in the mid–lower portion of the soil section with relatively weak development of net-like texture (Hong et al., 2012). However, in the lower soil profile intense hydromorphism occurred during the syndepositional pedogenesis, as indicated by the well-developed net-like texture. This would result in an environment with fluctuating base cation concentrations due to the poorly-drained conditions, and would favor the formation of metastable precursor mixed-layer clays (Thanachit et al., 2006). In hydromorphic circumstances the redox processes may influence the CEC and the swelling behaviour of clay minerals due to their effect on charge (Stucki, 2006). The changing layer charge will determine whether Ca^{2+} and Mg^{2+} ions enter into a structure providing a smectite mineral, or, where potassium is available in aqueous solutions, forming illite type minerals. In general, the high charge layers tend to attract either Al^{3+} ions or K^{+} ions, and the lower charge layers selectively adsorb divalent ions Ca^{2+} and Mg^{2+} (Stucki, 2006). These chemical forces will induce internal ionic migration and the clay particles may become internally heterogeneous (Velde and Meunier, 2010), and therefore can produce heterogeneous clay mineral layers in the crystallites, as observed by Eberl et al. (1986), who found heterogeneous

clay components of illite/vermiculite/smectite mixed-layer in crystallites.

The lower portion of the Xuancheng soils formed under seasonally dry humid tropical climatic conditions (Hong et al., 2010b), indicative of intense chemical weathering during the pedogenic modification of the sediments. The periodic redox processes may cause the incomplete transformation of inherited clay minerals during pedogenesis, and the newly formed metastable clay phases in association with the incompletely altered parent clays could simultaneously weather into stable species through subsequent chemical weathering. The presence of three component I/S/K mixed-layer clays in the soils suggested that transformations from illite to smectite and from smectite to kaolinite occurred simultaneously within a clay particle. The variable thickness observed in lattice fringe images from an illite layer to a smectite layer along a lattice fringe suggested that an interlayer ionic migration occurred during the alteration processes due to variations in charge (Figure 4d,e). Variations in layer charge have been observed to occur through chemical influences by internal ionic migration in smectite clays creating new charge sites in the structure without re-crystallization (Bauer et al., 2006). However, smectite to kaolinite transformation generally involves dissolution–precipitation reactions of a smectite layer within existing clay crystals. As shown in Figure 4d, a smectite layer changed laterally into a kaolinite layer. This suggested that the smectite layer dissolved progressively in a lateral manner as Al-rich, Si-poor fluids infiltrated into the interlayer along crystal edges (Ryan and Huertas, 2009). The transformation of smectite into kaolinite takes place through the progressive loss of the tetrahedral sheet of smectite layers, followed

by changes in the octahedral sheet and the remaining tetrahedral sheet (Dudek et al., 2006).

In situations where chemical leaching processes dominated, the transformations of the clay phases were governed by the mobility of the elements released by mineral dissolution (Rich, 1968). The stability of hydroxyl-aluminum species is pH-dependent (Churchman, 2000), and Al^{3+} cations could be produced by the destabilization of silicates including clay minerals in solutions with a pH≤6. It can be expected that, during the seasonal drying phase, hydrogen ions will become more concentrated in the soil solutions, thereby lowering their pH and increasing their solubility. Clay minerals show some increase in solubility as pH is decreased (e.g. Carroll and Starkey, 1971) and smectites, in particular release increasing amounts of Si, in addition to Al, to solution at low pH (Churchman and Jackson, 1976). Exposure of smectites to increasing acidic solutions as occurs with seasonal drying in these soils means that their tetrahedral layers which are adjacent to interlayers exposed to the solutions become more readily solubilised. In the lower soil profile, Al-rich and Si-poor aqueous solutions were readily produced by permeating groundwater with Al^{3+} dissolving from the upper soil profile due to intense chemical weathering, and the smectite to kaolinite transformation could be expected to occur as a result of the chemical composition of these aqueous solutions.

During weathering illite generally alters into smectite, vermiculite, and intermediate clay species (e.g., Churchman and Lowe, 2012). However, when the environment provides enough Al and Si in solution under acidic conditions, illite can alter to

kaolinite (Sand, 1956). As shown in Figure 4d, an illite layer was observed to laterally change into a kaolinite layer, indicating direct transformation from illite to kaolinite. The loss of tetrahedra produces domains of kaolinite structure in illite layers, but the layer will collapse to a 7 Å kaolinite layer only after the extent of the layers without two tetrahedra is sufficiently large. At a given alkali activity, change in illite mineral stability in favor of kaolinite may occur due to pH variation (Figure 6). In acidic conditions illite can transform into smectite (montmorillonite) in higher Si concentration solutions and into kaolinite in relatively lower Si concentration solutions during weathering. A seasonally dry and wet environment will cause the groundwater table to rise and fall frequently. Hydromorphism in the Xuancheng soil profile indicates fluctuating Si concentrations in solutions due to the seasonally varying climate, and thus caused both the illite to smectite and the illite to kaolinite transformations to occur in the pedogenic processes.

In Rio Grande do Sul State, Brazil under subtropical climate conditions, interstratified kaolinite-smectite and illite-smectite, illite, kaolinite, and hydroxy-aluminium interlayered vermiculite were observed in Acrisol soils in well-drained conditions (Bortoluzzi1 et al., 2008), where the intermediate species resulted from the transformation of inherited 2:1 clay minerals by intense leaching. However, the transformation of illite to kaolinite and to I/S/K three component mixed-layer clays occurred under subtropical climate conditions during the pedogenic processes in hydromorphic conditions in Xuancheng, mid-lower reaches of the Yangtze River,

CONCLUSIONS

XRD analysis and HRTEM observation showed that the most striking characteristic of clays found in Xuancheng hydromorphic soils is their uncommon intermediate behavior. In the XRD patterns, clay species were identified to be illite, kaolinite, smectite, and mixed-layer illite–smectite. However, HRTEM analysis suggested that 10 Å illite layers were interstratified with both 15 Å smectite layers and 7 Å kaolinite layers in clay grains, suggesting the occurrence of I/S/K three-component mixed-layer clays.

The lattice fringes of the I/S/K clays appeared corrugated and vanishing, and also showed variable thickness along a lattice fringe, in correspondence with illite to smectite, smectite to kaolinite, and illite to kaolinite transformations. In hydromorphic soils the redox processes may influence the CEC and the swelling behaviour of clay minerals due to variation in charge, and these chemical forces will induce internal ionic migration. The variable thickness in correspondence corresponding to transitions from illite layers to smectite layer suggested an interlayer ionic migration during the alteration processes. The smectite to kaolinite transformation appeared to occur through progressive dissolution in a lateral manner as Al-rich, Si-poor fluids infiltrated the interlayer along crystal edges. The lateral change from illite to kaolinite indicated direct transformation from illite to kaolinite by stripping tetrahedra from illite layers. In the Xuancheng soils fluctuating Al, Si concentrations and acidic solutions resulting from the concentration of hydrogen ions under seasonal drying in a

seasonally warm and humid climate has caused the transformation of illite to kaolinite through intermediate stages to occur by pedogenesis.

IMPLICATIONS

Clay minerals in soils may comprise complex mixtures of different types of aluminosilicate layers in interstratifications. This can arise because of seasonally changing hydromorphic conditions during soil formation. Redox changes that occur as a result can lead to variations in the charges on the layers. The chemistry of soil solutions, and particularly the nature of the cations surrounding the clay minerals and its pH can lead to changes within the interlayer that favor the occurrence of smectite (or vermiculite) or its reversion to an illitic phase. Depending on the relative activities of Al and Si ions and pH in the solutions, the transformation of illite to kaolinite can even occur by partial dissolution of the aluminosilicate layers due to increased acidity resulting from seasonal drying. The transformations of illite to smectite, vermiculite and kaolinite commonly occur via intermediate mixed-layer phases that can include any two, or even three of the component mineral types.

Acknowledgements

This work was supported by Natural Science Foundation of China (41272053 and 41472041) and the Specialized Research Fund for the Doctoral Program of Higher Education of China (20110145110001). The authors wish to thank Gu Y. S. for the sample preparation, Dr. Liu X. W. for the HRTEM observation, and Yu J. S. for the XRD analyses, and especially to Prof. Huff W. D., the Associate Editor, and the

anonymous reviewers for their insightful reviews, valuable comments and suggestions.

References

Allen, B.L., and Hajek, B.F. (1989) Mineral occurrence in soil environments. In J.B. Dixon and S.B. Weed, Eds., Minerals in Soil Environments, 2nd edition., p. 199–264, Soil Science Society of America, Madison, Wisconsin.

Bauer, A., Lanson, B., Ferrage, E., Emmerich, K., Taubald, H., Schild, D., and Velde, B. (2006) The fate of smectite in KOH solutions. American Mineralogist, 91, 1313–1322.

Bertsch, P.M. and Thomas, G.W. (1985) Potassium status of temperate region soils. In D.M Robert, Ed., Potassium in Agriculture, p. 201–276. American Society of Agronomy, Crop Science Society of America & Soil Science Society of America, Madison, Wisconsin.

Bhattacharyya, T., Pal, D.K., and Srivastava, P. (2000) Formation of gibbsite in the presence of 2: 1 minerals: an example from Ultisols of northeast India. Clay Minerals, 35, 827–840.

Bonifacio, E., Falsone, G., Simonov, G., Sokolova, T., and Tolpeshta, I. (2009) Pedogenic processes and clay transformations in bisequal soils of the SouthernTaiga zone. Geoderma, 149, 66–75.

Bortoluzzi1, E.C., Velde, B., Pernes, M., Dur, J.C., and Tessier, D. (2008) Vermiculite, with hydroxy-aluminium interlayer, and kaolinite formation in a

441 subtropical sandy soil from south Brazil. Clay Minerals, 43, 185–193.
442 Brinkman, R. (1970) Ferrolysis, a hydromorphic soil forming process. Geoderma, 3,
443 199–206.
444 Carroll, D., and Starkey, H.C. (1971) Reactivity of clay minerals with acids and
445 alkalis. Clays and Clay Minerals 19, 321–333.
446 Chesworth, W. (1992) Weathering systems. In I.P. Martini and W. Chesworth,
447 Eds.,Weathering, Soils and Paleosols, p. 19–40, Elsevier, Amsterdam.
448 Churchman, G.J. (1980) Clay minerals formed from micas and chlorites in some New
449 Zealand soils. Clay Minerals, 15, 59–76.
450 Churchman, G.J. (2000) The alteration and formation of soil minerals by weathering.
451 In M.E. Sumner, Ed., Handbook of Soil Science, p. F3–76, CRC Press, Boca Raton,
452 Florida.
453 Churchman, G.J., and Jackson, M.L. (1976) Reaction of montmorillonite with acid
454 aqueous solutions: solute activity control by a secondary phase. Geochimica et
455 Cosmochimica Acta, 40, 1521–1529.
456 Churchman, G.J., Lowe, D.J. (2012) Alteration, Formation and Occurrence of
457 Minerals in Soils. In P.M. Huang, Y. Li and M.E. Sumner, Eds., Handbook of Soil
458 Sciences, 2nd edition, Properties and Processes, p. 20.1–20.72, CRC Press, Boca
459 Raton, Florida.
460 Churchman, G.J., Pontifex, I.R., McClure, S.G. (2010) Factors affecting the formation
461 and characteristics of halloysites or kaolinites in granitic and tuffaceous saprolites
462 in Hong Kong. Clays and Clay Minerals, 58, 220–237.

463 Cradwick, P.D. and Wilson, W.J. (1978) Calculated x-ray diffraction curves for the
464 interpretation of a three-component interstratified system. Clay Minerals, 13, 53-65.
465 Deconinck, J.F. and Chamley, H. (1995) Diversity of smectite origins in late
466 Cretaceous sediments: Example of chalks from northern France. Clay Minerals, 30,
467 365–379.
468 Dudek, T., Cuadros, J., and Fiore, S. (2006) Interstratified kaolinite-smectite: Nature
469 of the layers and mechanism of smectite kaolinization. American Mineralogist, 91,
470 159–170.
471 Dumon, M., Tolossa, A.R., Capon, B., Detavemier, C., and Van Ranst, E. (2014)
472 Quantitative clay mineralogy of a vertic planosol in southwestern Ethiopia: Impact
473 on soil formation hypotheses. Geoderma, 214, 184–196.
474 Eberl, D.D., Srodon, J., and Northrop, H.R. (1986) Potassium fixation in smectite by
475 wetting and drying. In J.A. Davis, K.F. Hayes, Eds., Geochemical Processes at
476 Mineral Surfaces. ACS Symposium Series, 323, p. 296–326. American Chemical
477 Society, Washington, D C.
478 Garrels, R.M. (1984) Montmorillonite/illite stability diagrams. Clays and Clay
479 Minerals, 32, 161–166.
480 Gu, Y.P., Qian, J., Lv, C.W., Liu, F.C., Wei, X., Jia, H.J., 2001. Classification of soil
481 series in Xuancheng, Anhui. Soils, 33 (1), 7–12 (in Chinese).
482 Guthrie, G. D, and Veblen, D. R. (1989) High-resolution transmission electron
483 microscopy of mixed-layer illite/smectite: computer simulations. Clays and Clay
484 Minerals, 37, 1–11.

Han, W., Hong, H.L., Yin, K., Churchman, G.J., Li, Z. and Chen, T. (2014) Pedogenic alteration of illite in subtropical China. Clay Minerals, 49, 391–402.

Herbillon, A.J., Frankart, R., and Vielvoye, L. (1981) An occurrence of interstratified kaolinite–smectite minerals in a red–black soil toposequence. Clay Minerals, 16, 195–201.

Hong, H.L., Wang, C.W., Zeng, K.F, Gu, Y.S., Wu, Y.B., Yin, K., and Li, Z. (2013) Geochemical constraints on provenance of the mid-Pleistocene red earth sediments in subtropical China, Sedimentary Geology, 290, 97–108.

Hong, H.L., Gu, Y.S., Li, R.B., Zhang, K.X., and Li, Z. (2010) Clay Mineralogy and Geochemistry and their Palaeoclimatic Interpretation of the Pleistocene Deposits in the Xuancheng Section, South China. Journal of Quaternary Science, 25(5), 662–674.

Hong, H.L., Churchman, G.J., Gu, Y.S., Yin, K., and Wang, C.W. (2012) Kaolinite–smectite mixed-layer clays in the Jiujiang red soils and their climate significance. Geoderma, 173–174, 75–83.

Hong, H.L., Churchman, G.J., Yin, K., Li, R.B., and Li, Z. (2014) Randomly interstratified illite–vermiculite from weathering of illite in red earth sediments in Xuancheng, southeastern China. Geoderma, 214-215, 42–49.

Hu, X.F., Gong, Z.T., Xia, Y.F., Sui, Y.X., Du, J.H. (1999) Comparative study of yellow-brown earth and Quaternary red clay in Xuanzhou, Anhui province and its palaeoclimate significance. Acta Pedologica Sinica, 36(3), 301–307 (Chinese text with English abstract).

Hubert, F., Caner, L., Meunier, A., and Ferrage, E. (2012) Unraveling complex < 2 μm clay mineralogy from soils using x-ray diffraction profile modeling on particle-size subfractions: Implications for soil pedogenesis and reactivity. American Mineralogist, 97, 384–398.

Ismail, F.T. (1970) Biotite weathering and clay formation in arid and humid regions, California. Soil Science, 109, 257–261.

Jackson, M.L. (1978) Soil Chemical Analysis. Published by the Author, University of Wisconsin Madison, USA.

Laird, D.A. and Nater, E.A. (1993) Nature of the illitic phase associated with randomly interstratified smectite/illite in soils. Clays and Clay Minerals, 41(3), 280–287.

Li, C.A. and Gu, Y.S. (1997) Stratigraphic study on the vermicular red earth at Xiushui county, Jiangxi province. Journal of Stratigraphy, 21, 226–232. (Chinese text with English abstract).

Nahon, D. (1991) Introduction to the petrology of soils and chemical weathering. John Wiley and Sons, New York, 313 pp.

Ryan, P.C., and Huertas, F.J. (2009) The temporal evolution of pedogenic Fe–smectite to Fe–kaolin via interstratified kaolin–smectite in a moist tropical soil chronosequence. Geoderma 151, 1–15.

Rich, C.I. (1968) Hydroxy interlayers in expansible layer silicates. Clays and Clay Minerals, 16, 15–30.

Sakharov, B.A., Lindgreen, H., Salyn, A.L., and Drits, V.A. (1999) Mixed-layer

kaolinite-illite-vermiculite in north sea shales. Clay Minerals, 34, 333–344.

Sand, L.B. (1956) On the genesis of residual kaolins. American Mineralogist, 41, 28–40.

Singer, A. (1980) The paleoclimatic interpretation of clay minerals in soils and weathering profiles. Earth Science Reviews, 15, 303–326.

Stucki, J.W. (2006) Properties and behavior of iron in clay minerals. In: Bergaya, F., Theng, B. K.G., Lagaly, G. (Eds.), Handbook of Clay Science. Elsevier, Amsterdam, pp. 423–475.

Thanachit, S., Suddhiprakarn, A., Kheoruenromne, I., Gilkes, R.J. (2006) The geochemistry of soils on a catena on basalt at Khon Buri, northeast Thailand. Geoderma, 135, 81–96.

Van Der Gaast, S.J., Mizota, C., Jansen, J.H.F. (1986) Curved smectite in soils from volcanic ash in Kenya and Tanzania: a low-angle x-ray powder diffraction study. Clays and Clay Minerals, 34 (6), 665–671.

Velde, B. and Meunier, A. (2010) The Origin of Clay Minerals in Soils and Weathered Rocks, Springer-Verlag Berlin, Heidelberg, 406 pp.

Wilson, M.L. (1987) Soil smectites and related interstratified minerals: recent developments. In L.G. Shultz, H. van Olphen, and F.A. Mumpton, Eds., Proceedings of the International Clay Conference, Denver, 1985, p. 167–173, Clay Minerals Society, Bloomington, Indiana.

Wilson, M.J. (2004) Weathering of the primary rock-forming minerals: processes, products and rates. Clay Minerals 39, 233–266.

Yin, K., Hong, H.L., Churchman, G.J., Li, R.B., Li, Z., Wang, C.W., and Han, W. (2013) Hydroxy-interlayered vermiculite genesis in Jiujiang late-Pleistocene red earth sediments and significance to climate. Applied Clay Science, 74, 20–27.

Yin, Q.Z., Guo, Z.T., Fang, X.M. (2006) Micromorphology of latosols in Hainan and differences between vemiculated red soils and latosols in environmental significance in south China. Acta Pedologica Sinica, 43(3), 353–361 (Chinese text with English abstract).

Zhao Q, Yang H. 1995. A preliminary study on red earth and changes of Quaternary environment in south China. Quaternary Sciences, 15:107–115 (Chinese text with English abstract).

Zhu, J.J. (1988) Genesis and research significance of the plinthitic horizon. Geographical Research, 7, 12–20 (Chinese text with English abstract).

Zhu, L.D. (2007) Aggradation red earth sediments in mid-subtropics of China and their recorded environmental changes during Quaternary. Ph. D. Dissertation, Lanzhou University, p.p. 156 (Chinese text with English abstract).

Table 1 The physical and chemical properties of the studied soils

Soil taxonomy	CEC (cmol/kg)	pH	Particle size distribution (%)			Organic matter content (wt%)
			>63μm (sand)	63-4 μm (silt)	<4μm (clay)	
Oxisols	10.3±0.6	4.91±0.05	0.10	69.68	30.22	0.294±0.087

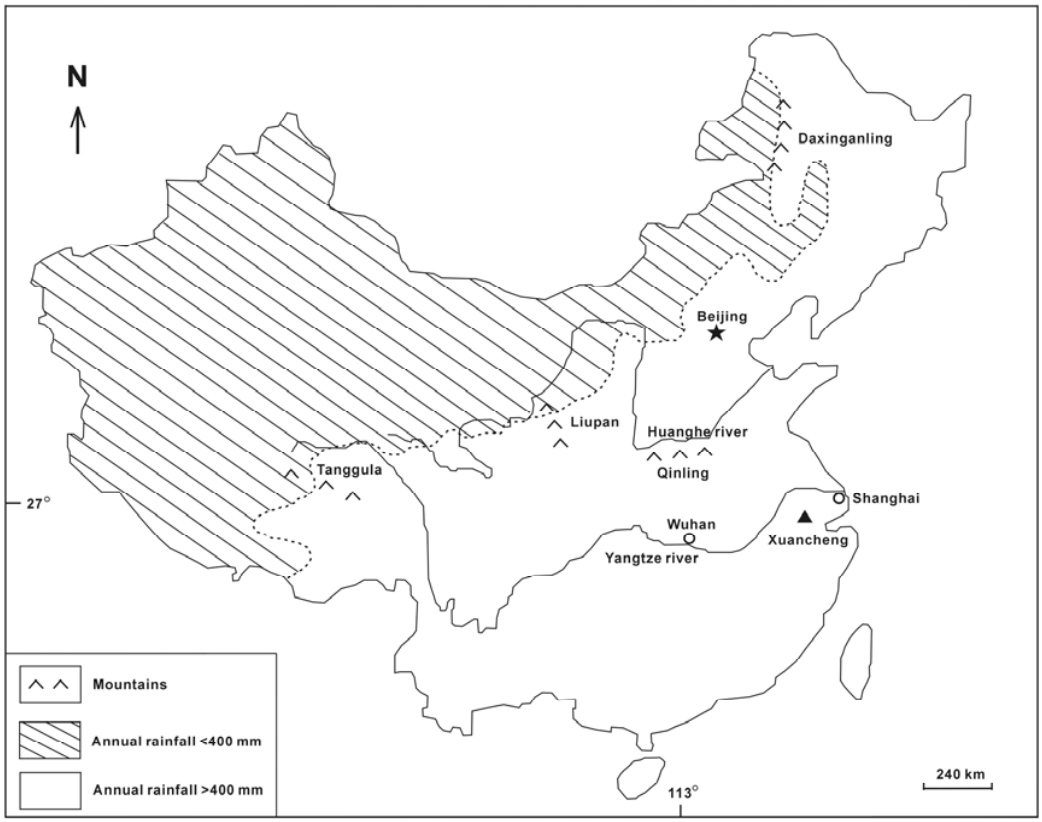

Figure 1 A generalized map showing the location of the study area.

Figure 2 (a) A full view of the soil profile showing the occurrence of well-developed net-like veins in the lower section

Figure2 (b) A close-up photograph showing the shape and size of the net-like veins (Pen length 15 cm)

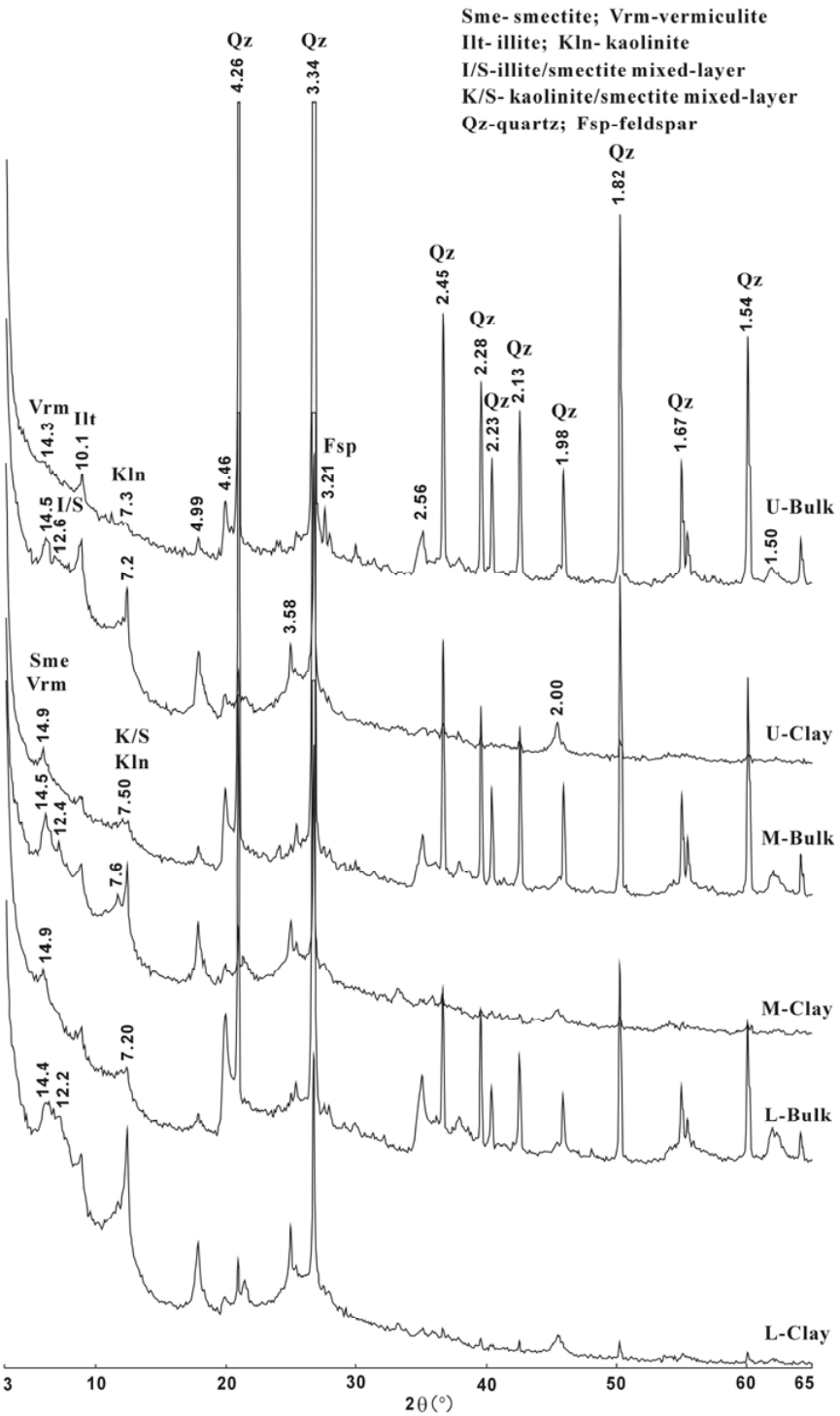

Fig 3a The XRD patterns of samples showing the mineral composition of the soil profile. XRD experimental patterns are powders, and samples are natural without saturation. U-Bulk: Bulk sample from the upper portion; U-Clay: Clay fraction of soil from the upper portion; M-Bulk: Bulk sample from the middle portion; M-Clay: Clay fraction of soil from the middle portion; L-Bulk: Bulk sample from the lower portion; L-Clay: Clay fraction of soil from the lower portion.

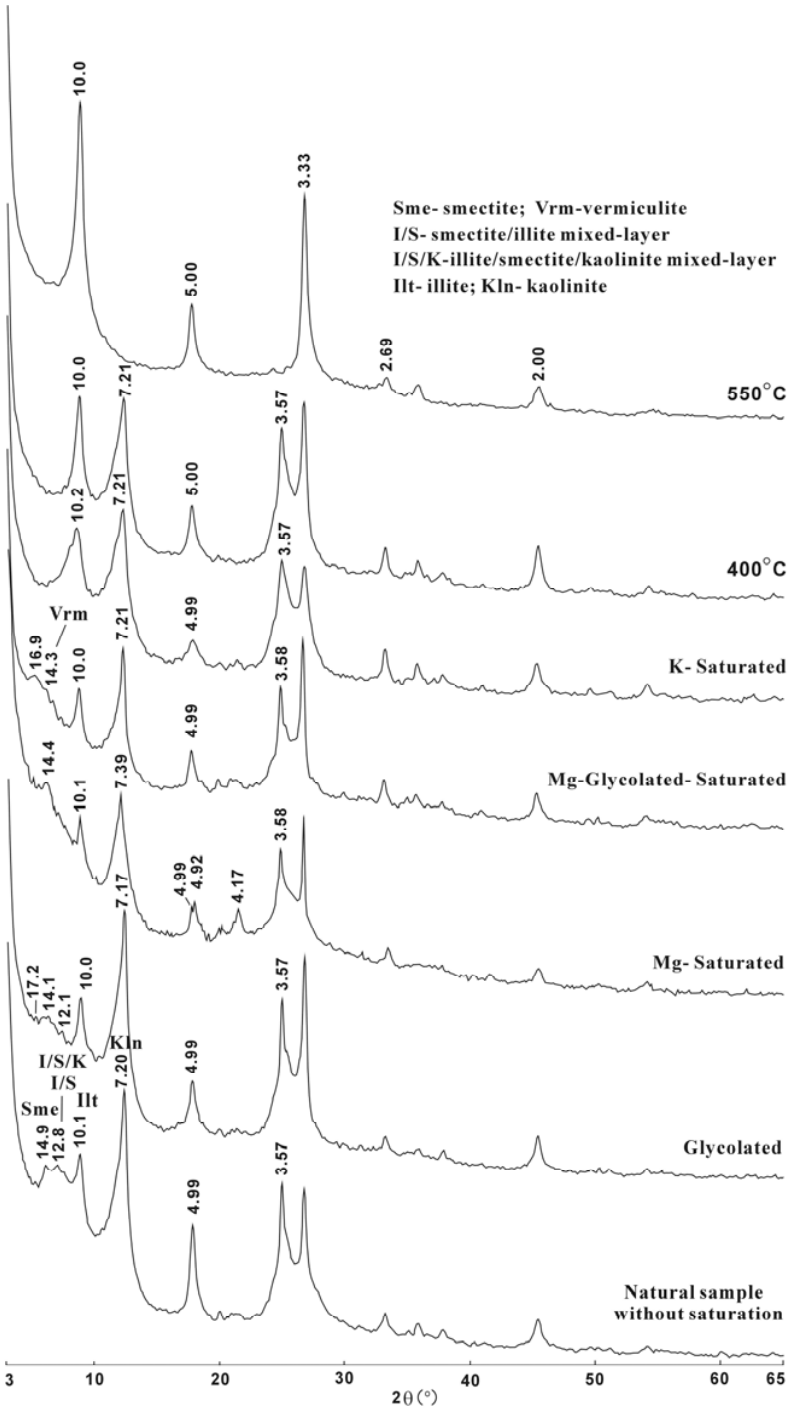

Figure 3b The XRD patterns of samples from the lower portion with a distinct white net-like structure showing the mineral composition of the hydromorphic soil. Natural sample without saturation: oriented sample dried at ambient temperature; Glycolated: ethylene glycol saturation; K-Saturated: exchanged by K^+ solution; 400° C: heated to 400 ° C; 550° C: heated to 550° C.

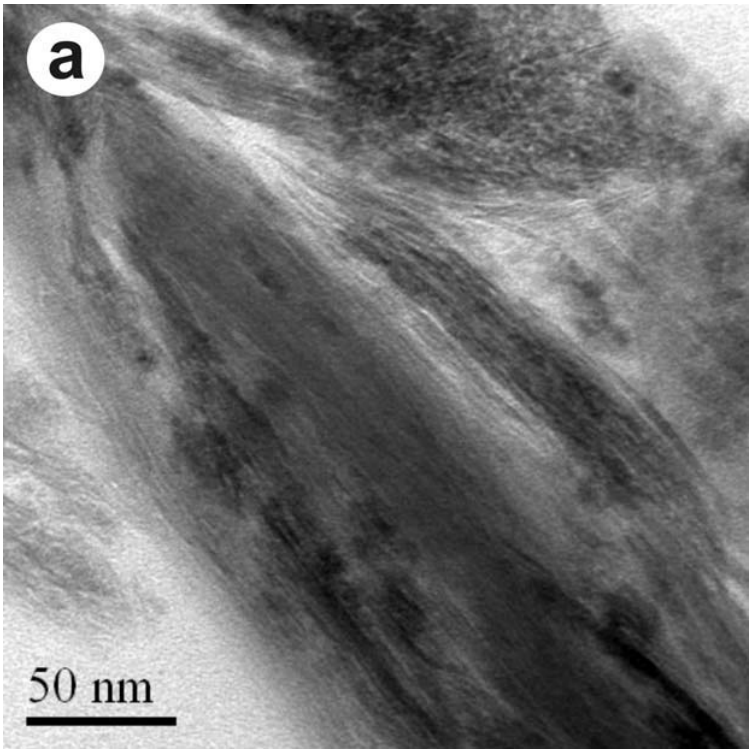

Figure 4 HRTEM images of the Xuancheng soil. (a) Smectite and mixed-layer illite-smectite showing the characteristic wave–shaped morphology

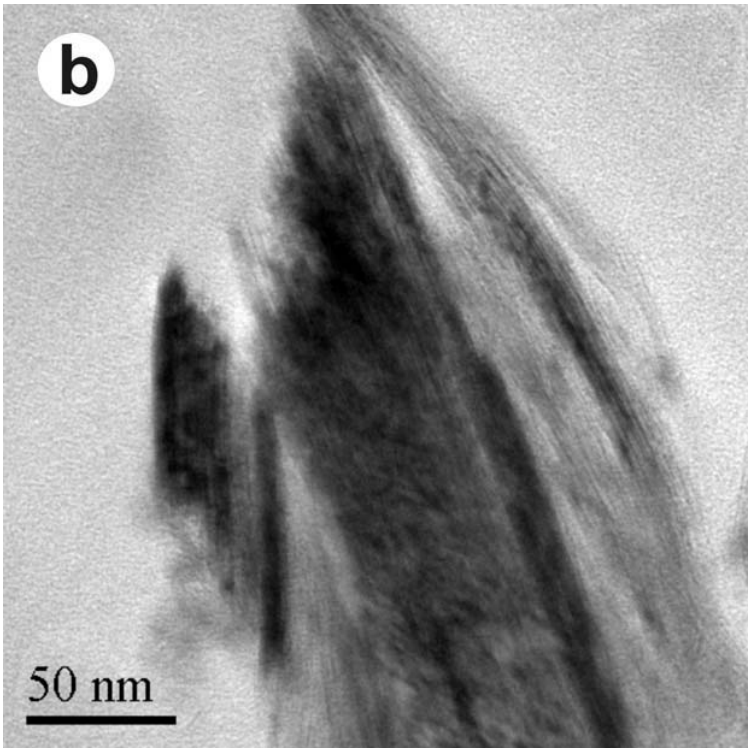

Figure 4 (b) Clay particles in aggregates with irregular outline

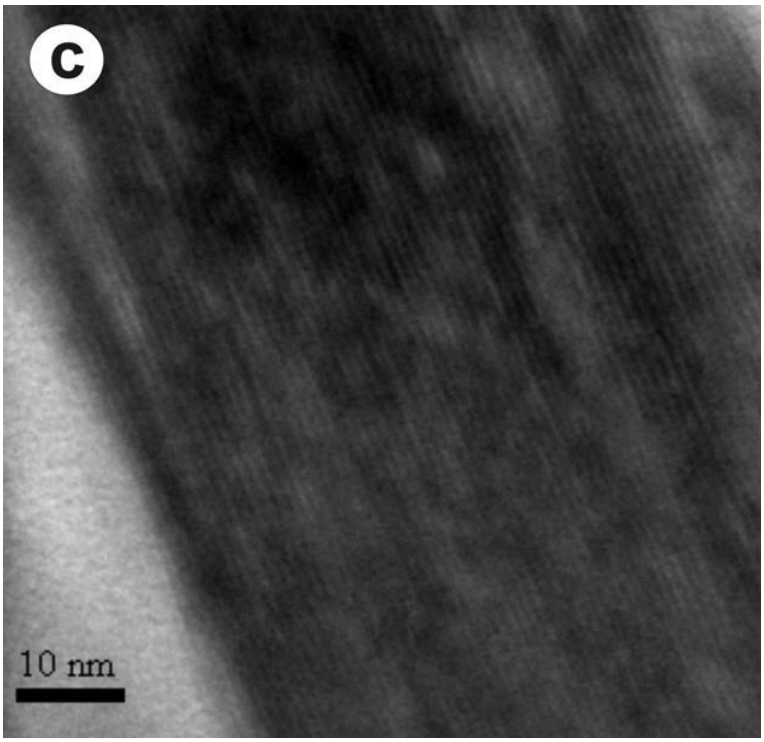

Figure 4 (c) Illite in relatively thick and plate-shaped outline with straight lattice fringes of 10 Å spacing

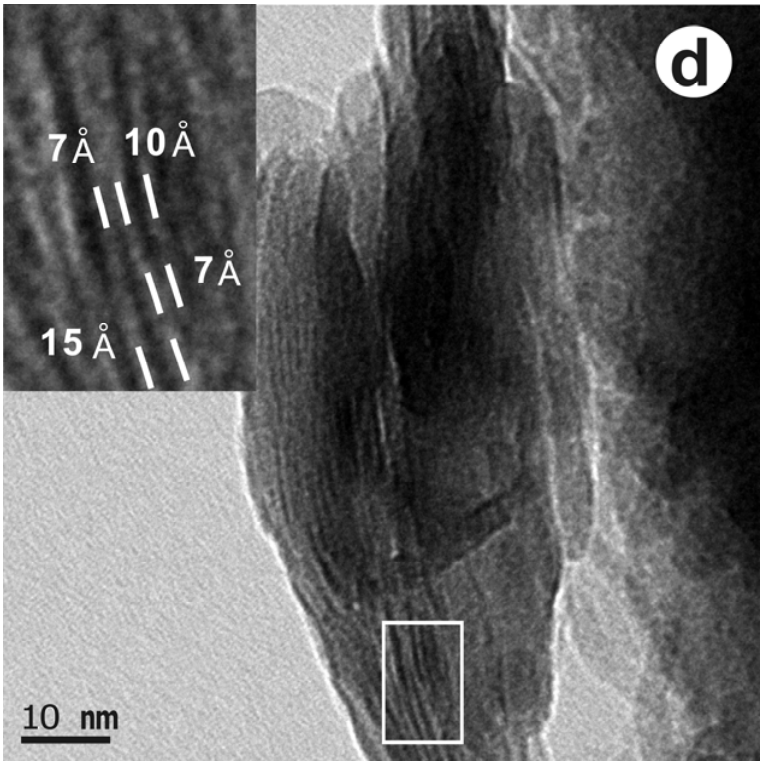

Figure 4 (d) Lateral transition from illite layer to kaolinite layer and from smectite layer to kaolinite layer

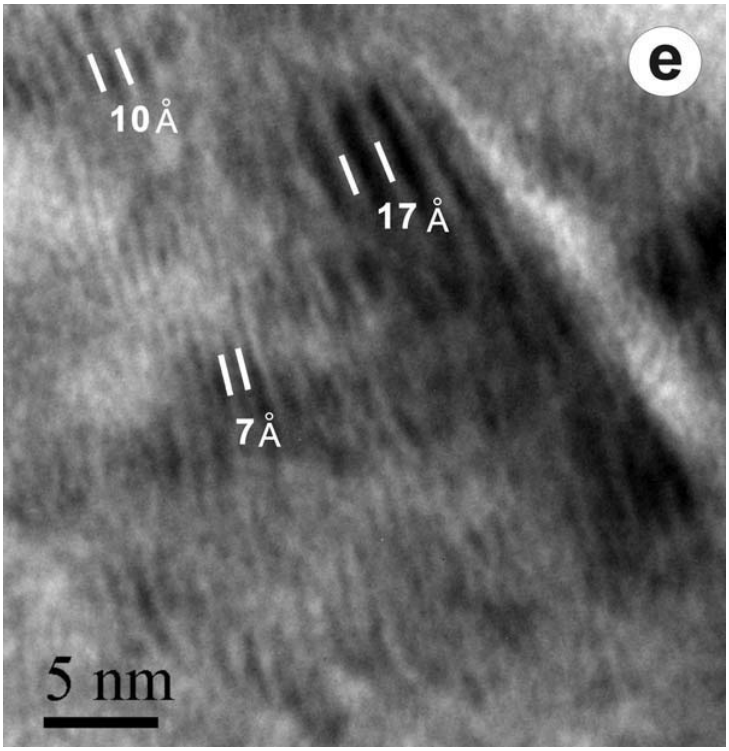

Figure 4 (e) The interstratified 10, 17, and 7 Å layers in clay crystallites of a glycolated sample.

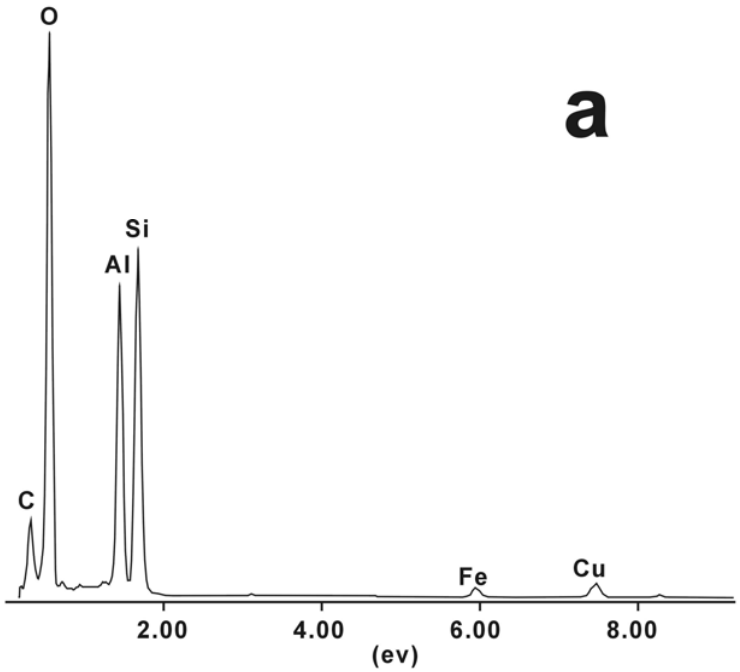

Figure 5 The EDS spectra of the interstratified clay crystallites (a) The 7 Å domain

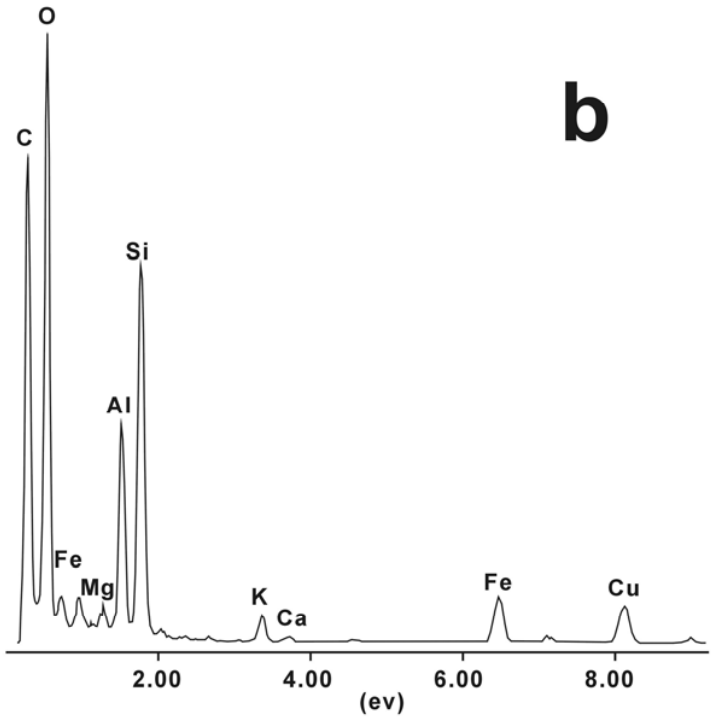

Figure 5 The EDS spectra of the interstratified clay crystallites (b) The 10 Å domain

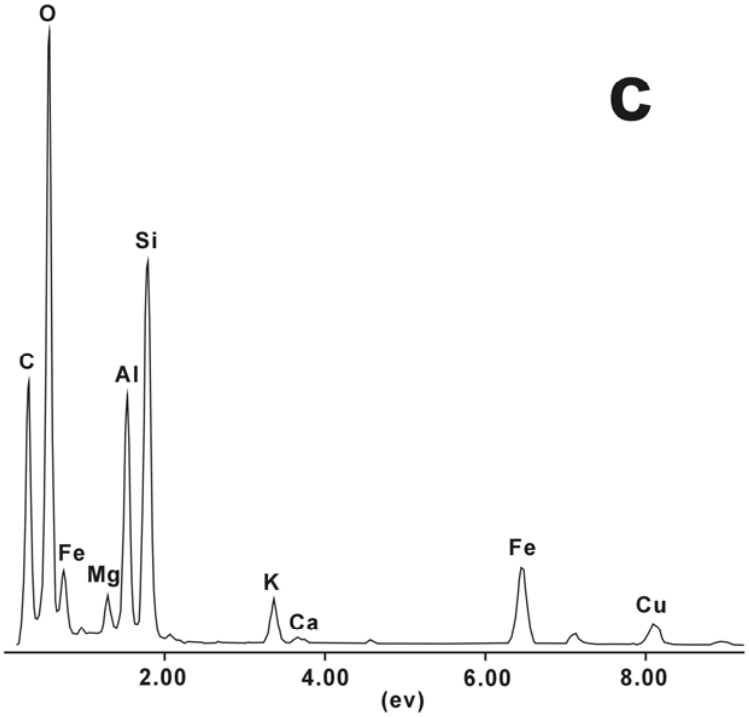

Figure 5 The EDS spectra of the interstratified clay crystallites (c) The 15 Å domain

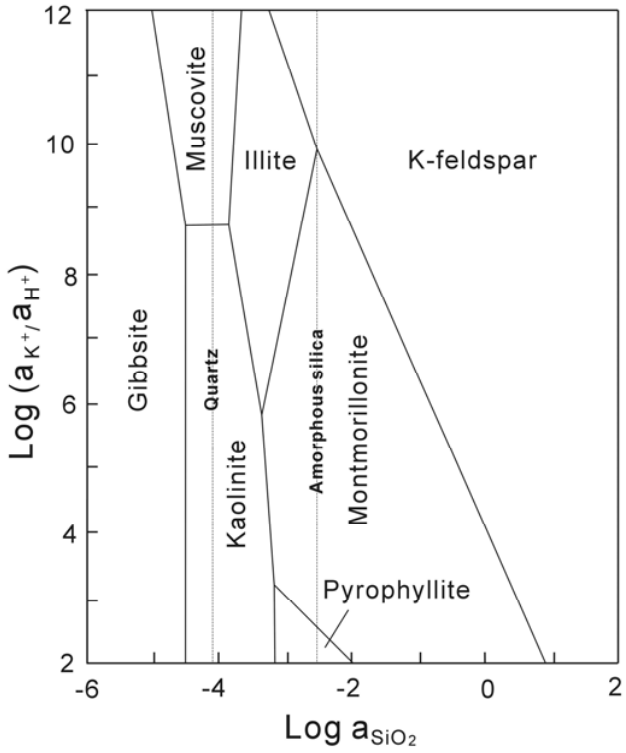

Figure 6 The illite/smectite/kaolinite stability diagrams (adapted from Garrels, 1984)